iomac
International Operational Modal Analysis Conference
11th International Operational Modal Analysis Conference
20 - 23 May 2025 | Rennes, France

Reliable damping ratio estimates from a 50m+ wind turbine rotor blade as a guide for prototype testing in the low frequency regime

Yves Govers[1,*], *Kevin Gnebner*[1], *Philipp Kober*[1] *and Giulia Jelicic*[1]

[1] German Aerospace Center (DLR), Institute of Aeroelasticity, Bunsenstraße 10, 37073 Göttingen, Germany
[*] Corresponding author: yves.govers@dlr.de

ABSTRACT
The accurate damping estimation is of great importance for the design and validation of wind turbine rotor blades.
We present experimental and operational modal analysis results conducted on a large wind turbine blade using a novel procedure that can reduce testing time and equipment.
Reference modal parameters were obtained by a hammer test. Afterwards, the eigenfrequency and damping ratio were estimated by a free-decay test. This was performed by harmonically exciting the rotor blade by hand until large amplitudes were achieved, after which the oscillations were left to decay.
We show that the estimated modal parameters are a function of oscillation amplitude. The experiment was conducted for the first three out-of-plane and for the first two in-plane rotor blade bending modes. The damping ratio increases with oscillation amplitude, while the eigenfrequency is only minimally affected. The test requires only limited equipment and simple algorithms.

Keywords: wind turbine testing; operational modal analysis; damping estimation

1. INTRODUCTION

Modal testing is performed on wind turbine rotor blades to understand their dynamic behaviour and ensure their structural integrity under various operating conditions. Modal testing may be conducted to improve damage detection, fatigue life assessment, design optimization, operational stability, control system tuning. An accurate damping estimation is necessary for effective design and operation. Depending on testing scope, this may involve complex sensor setups [1][2].

This article contributes to experimental procedures in modal analysis by investigating the amplitude-dependent eigenfrequency and damping ratio of a wind turbine rotor blade. This procedure can be performed as prototype testing in the later stages of the blade manufacturing process. The procedure has the advantage of low requirement for equipment and analysis methods.

The paper is structured as follows: experimental setup (section 2.), experimental procedure (section 3.), analysis methods (section 4.), results (section 5.), conclusions (section 6.).

2. EXPERIMENTAL SETUP

The tested rotor blade is a prototype with the tip sawed off. Its total length is 50.5 m. The rotor blade is cantilevered firmly at its root on an indoors test rig. The blade geometry, reference coordinate system and sensor positions are displayed in figure 1. The reference directions are: out-of-plane (x), in-plane (y) and axial (z). Ten triaxial MEMS accelerometers are mounted along equidistant stations on the upper surface along the rotor blade's axis. Furthermore, seven ICP accelerometers (six in the x-direction and one in the y-direction) are placed on the some of the stations as shown in the right subplot of figure 1. This setup was originally meant to compare different sensor systems; during the test additional data were acquired to validate the simple and reliable damping ratio estimation procedure presented here.

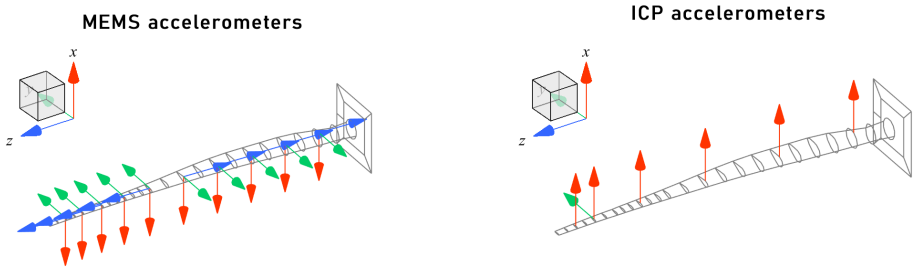

Figure 1: Sensor setup for modal testing for the MEMS and ICP accelerometers.

3. EXPERIMENTAL PROCEDURE

The modal test presented in this article consists of three approaches:

1. Ambient excitation (OMA)
2. Hammer test (EMA)
3. Free-decay (OMA)

The ambient excitation and the hammer test data sets are characterized by low overall amplitudes. On the other hand, much larger vibration amplitudes are achieved in the free-decay test.

3.1. Ambient excitation

The sensor setup was first checked by analysing the response to ambient excitation acting on the rotor blade (data acquired during a lunch break). This data record consists of about 20 minutes of stationary ambient excitation, which is appropriate for a structure with such low eigenfrequency and damping. The corresponding modal analysis results are presented in section 5.1.

3.2. Hammer test

A standard hammer test (impact excitation) procedure was performed to obtain reference modal data. The impulse was applied at two locations towards the tip in the x and y directions in order to excite well both the out-of-plane and the in-plane bending modes. A picture of the modal hammer is available in figure 2. The hammer test results are found in section 5.2.

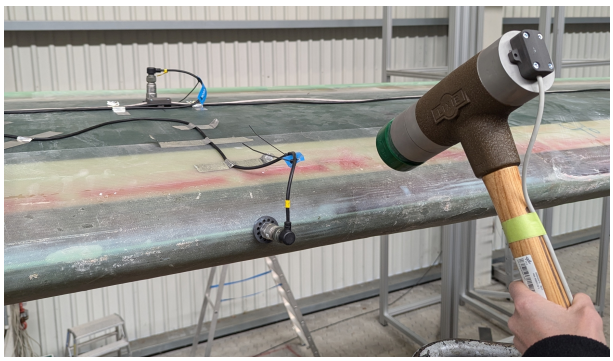

Figure 2: Impact hammer during modal testing. The rotor blade and two sensors are visible.

3.3. Free-decay test

The free-decay modal test is carried out as follows:

1. *Ramp-up phase*: the experimenter excites the structure harmonically by hand near or at resonance. The vibration amplitude increases for the excited eigenmode, while the others decay. A metronome may be set up to provide the correct beat. It is also possible to feel the right frequency by touch.

2. *Free-decay phase*: once the desired vibration amplitude is reached, the vibration is left to decay. By now the vibration should be predominantly mono-component on all sensors.

The free-decay experimental procedure is illustrated in figure 3 and estimates a single eigenmode per record. The size of the rotor blade leads to low eigenfrequencies that can excited by hand. We present the results in section 5.3.

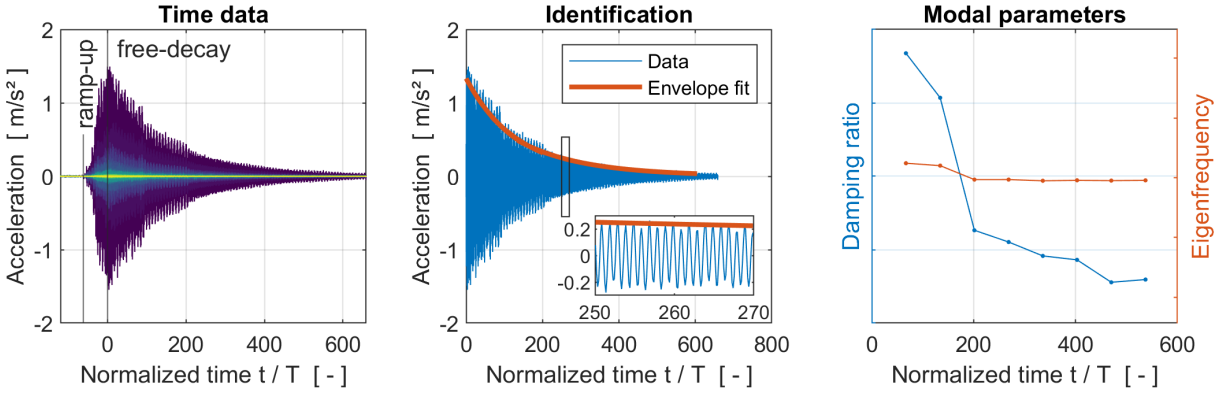

Figure 3: Experimental procedure for the free-decay test. The time axis is normalized by the oscillation period. Left: one eigenmode is excited till large amplitudes are achieved and then left to decay. Centre: signal processing. Right: modal parameters estimation.

4. ANALYSIS METHODS

For the ambient excitation and free-decay cases, the modal parameters are estimated with the methods of operational modal analysis (OMA). The hammer test is conducted within the experimental modal analysis (EMA) framework in frequency-domain. In this investigation the following methods are employed for system identification: SSI: *stochastic subspace identification* (OMA), LSCF: *least-squares complex frequency* (EMA), LogDec: *logarithmic decrement* (OMA).

4.1. Stochastic subspace identification (SSI)

The Stochastic Subspace Identification (SSI) method is the most commonly used output-only algorithm for operational modal analysis. The mathematical details are found in [3] and the references therein. The model structure is a discrete-time state-space model:

$$\begin{aligned} \mathbf{x}_{n+1} &= \mathbf{A}\mathbf{x}_n + \mathbf{w}_n \\ \mathbf{y}_n &= \mathbf{C}\mathbf{x}_n + \mathbf{v}_n \end{aligned} \tag{1}$$

where $\mathbf{y}_n$ are the measured outputs, $\mathbf{x}_n$ the system states, $\mathbf{A}$ the state matrix, $\mathbf{C}$ the output matrix. $\mathbf{w}_k$ and $\mathbf{v}_k$ are assumed white noise terms. SSI estimates the state and output matrices, from which the eigenvalues and eigenmodes are then calculated. We use the data-driven SSI with unweighted principal component (UPC) algorithm; the modal parameter variance is estimated as detailed in [4].

4.2. Least-squares complex frequency (LSCF)

Frequency-domain system identification is performed with the polyreference LSCF algorithm. The LSCF model structure is a frequency response function in polynomial form:

$$\mathbf{H}(z) = \frac{\sum_{n=0}^{N_m} \mathbf{B}_n z^n}{\sum_{n=0}^{N_m} \mathbf{a}_n z^n} = \sum_{k=1}^{N_m} \frac{\boldsymbol{\psi}_k \boldsymbol{\phi}_k^T}{z - \lambda_k} \tag{2}$$

where N_m is the model order for the nominator and denominator. The system poles λ_k are the roots of the denominator. The eigenmodes $\boldsymbol{\psi}_k$ and modal participation factors $\boldsymbol{\phi}_k$ are fitted in a second step using the LSFD algorithm to obtain the modal form of the transfer function. A more detailed description of the LSCF + LSFD identification method is found in [5][6].

4.3. Logarithmic decrement (LogDec)

SSI and LSCF are well-established in the multiple-input-multiple-output (MIMO) framework, both for OMA and for EMA. On the other hand, the logarithmic decrement (LogDec) method is valid for a single-degree-of-freedom system. However, under certain conditions, it may be used for systems with multiple degrees of freedom: for instance in [7] it is applied together with band-pass filtering to isolate the modes, while in [8] it is applied to determine the aerodynamic damping on oscillating cantilever beams.

In our investigation we apply the logarithmic decrement to the free-decay response of the rotor blade. During the ramp-up phase the system is excited at one frequency and if the modes are well-separated, the resulting response is predominantly mono-component (for this structure this is indeed the case). We may therefore write the response signal for an arbitrary output as:

$$y(t) = A_0 \mathrm{e}^{-\delta t} \cos(\omega_d t + \phi_0) \tag{3}$$

where A_0 is the amplitude, δ the decay rate, ω_d the oscillation frequency and ϕ_0 a phase. It is then possible to estimate the modal parameters using the logarithmic decrement applied to the signal's envelope [9]. We can use the Hilbert transform $\mathcal{H}\{\cdot\}$

$$y'(t) \triangleq \mathcal{H}\{y(t)\} \equiv \frac{1}{\pi t} * y(t) \qquad \Longrightarrow \qquad \tilde{y}(t) \triangleq y(t) + \mathrm{i}y'(t) \quad \in \mathbb{C} \tag{4}$$

to obtain the signal's analytic representation $\tilde{y}(t)$. The signal envelope is given by $|\tilde{y}(t)|$. For our analysis we select the signal with the best signal-to-noise ratio and downsample it to include the maximal frequency of interest ($f_{max} = 1.8$ in scaled units) in order to eliminate high-frequency noise contributions to the envelope.

From equations (3) and (4) we then see that

$$\ln|\tilde{y}(t)| = \ln A_0 - \delta t \qquad \angle\tilde{y}(t) = \omega_d t + \phi_0 \tag{5}$$

The four unknowns A_0, δ, ω_d and ϕ_0 can be estimated from the $\tilde{y}(t_1), \tilde{y}(t_2), \ldots, \tilde{y}(t_N)$ samples in each data block using a linear least-squares fit:

$$\begin{bmatrix} \ln|\tilde{y}(t_1)| & \angle\tilde{y}(t_1) \\ \ln|\tilde{y}(t_2)| & \angle\tilde{y}(t_2) \\ \vdots & \vdots \\ \ln|\tilde{y}(t_N)| & \angle\tilde{y}(t_N) \end{bmatrix} = \begin{bmatrix} 1 & t_1 \\ 1 & t_2 \\ \vdots & \vdots \\ 1 & t_N \end{bmatrix} \begin{bmatrix} \ln A_0 & \phi_0 \\ -\delta & \omega_d \end{bmatrix} \tag{6}$$

The eigenfrequency (in rad/s) and damping ratio are then respectively:

$$\omega_n = \sqrt{\omega_d^2 + \delta^2} \qquad \zeta = \delta/\omega_n \tag{7}$$

It will be shown in the results' section, that the logarithmic decrement method delivers estimates in line with more sophisticated system identification algorithms.

5. RESULTS

The modal analysis results for the ambient excitation §3.1., the hammer test §3.2. and the free-decay test §3.3. are presented in this section. The eigenfrequency and damping ratio are scaled by an undisclosed factor due to confidentiality.

We focus on the first five eigenmodes of the rotor blade: the first three flap-wise (out-of-plane) and the first two edge-wise (in-plane) bending modes. The flap modes are dominant in the x-direction, while the edge modes are dominant in the y-direction. The identified eigenmodes are shown in figure 4.

5.1. Ambient excitation

The ambient excitation data (see section 3.1.) was analysed in the OMA framework. Figure 5 displays the autopower spectral density of the ICP accelerometers, with the color denoting the direction. The first five eigenmodes are visible. The spectra show that the x-direction accelerometers have better signal-to-noise ratio for the out-of-plane bending modes (respectively: the y-direction accelerometers for in-plane bending modes). The modal analysis results for ambient excitation are shown in figure 6. System identification has been performed by the data-driven SSI algorithm with variance estimation as described in section 4.1. The analysis shows that the coefficient of variation (CV) of the estimated modal parameters is low. The eigenmodes are well-separated. Results are summarised in table 1.

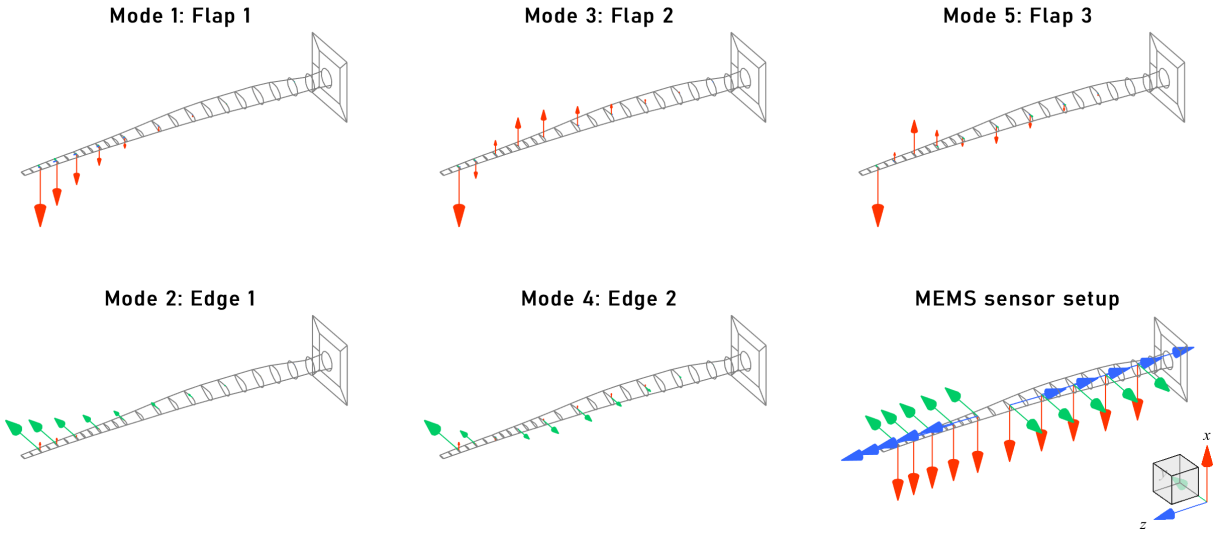

Figure 4: Identified eigenmodes: first, second and third flap-wise (out-of-plane) bending modes, and first and second edge-wise (in-plane) bending modes. The sensor setup is displayed in the bottom right subplot.

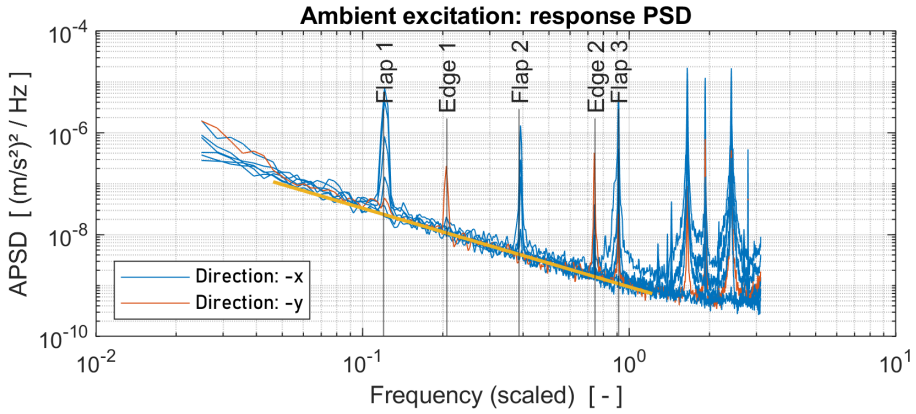

Figure 5: Ambient excitation: autopower spectra density of the response signals. The first five eigenmodes are highlighted. The thick yellow line is the fitted noise floor $G_n(\omega) \propto \omega^{-8/5}$.

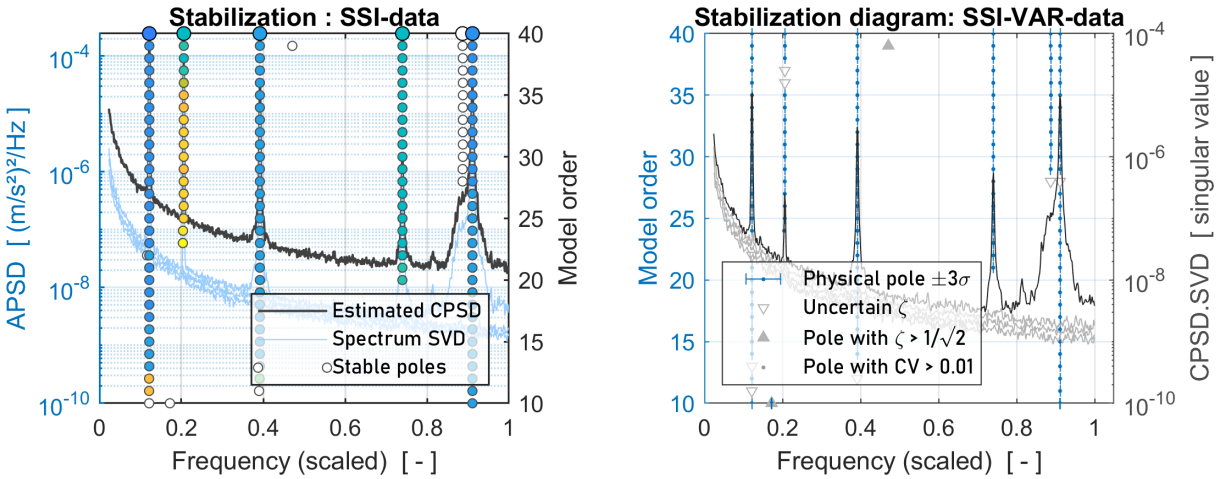

Figure 6: Ambient excitation stabilization diagrams (data-driven SSI). The identified modal parameters are presented in two plots. Left: stable poles with color-coded damping (blue: low, yellow: high, white: out-of-range). Right: stabilization diagram with error bars displaying the estimated eigenfrequency variance for each pole.

5.2. Hammer test

Hammer test data is identified from estimated frequency response functions (FRF) using the polyreference LSCF algorithm. A force window is applied to the force signal to eliminate any hits the hammer may have registered by handling it while waiting for the excitation to decay completely. At least ten impulses with sufficient bandwidth and without double hits are averaged to obtain frequency response estimates suitable for modal analysis. The frequency response has been estimated by the H_1-estimator. The stabilization diagram of the hammer test is displayed in figure 7. We see that the reconstructed frequency response is in very good agreement with measurements. The estimated modal parameters are compared to the ambient excitation test in table 1. Despite using different estimation frameworks, the eigenfrequencies agree completely, while the damping ratio displays small differences.

5.3. Free-decay

For the free-decay test the structure was excited by hand by the experimenter as described in section 3.3.. The first three flap modes (out-of-plane bending) and the first two edge modes (in-plane bending) could be excited this way. Higher eigenmodes are progressively harder to excite because they require frequencies that are difficult for the experimenter to achieve and maintain consistently.

Plotting the free-decay data in a log-log plot reveals that the decay rate is not constant (the oscillation maxima do not lie on a straight line). This indicates that the system is not time-invariant and its modal

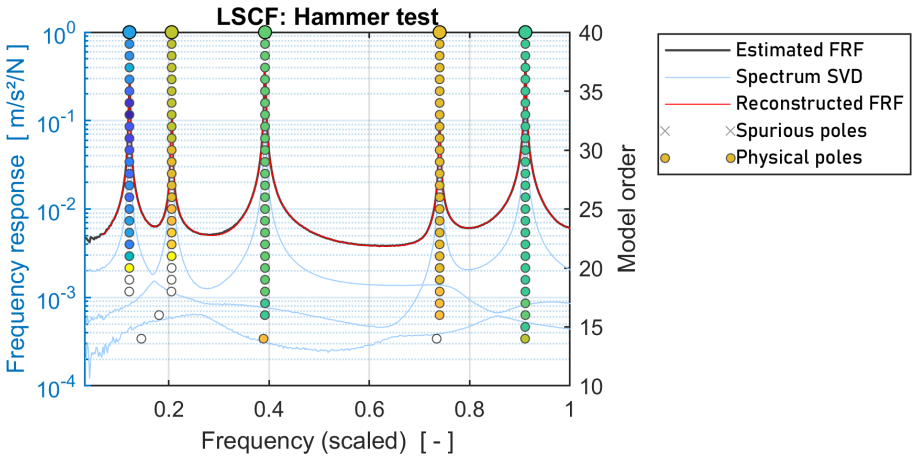

Figure 7: Hammer test stabilization diagram. The identified eigenfrequencies are denoted by markers. The marker color represents the damping ratio (blue: low, yellow: high, white: out-of-range). The black line is the sum of the (nonparametric) FRF estimates. The light blue curves are the singular values of the input spectra. The red curve is the sum of the identified (parametric) frequency response.

parameters are amplitude-dependent. During the free-decay runs, the maximal deflection at the tip from the rest position relative to the total length of the rotor blade was $\delta_{flap} = 0.35/50.5 = 0.0069$ and $\delta_{edge} = 0.15/50.5 = 0.0030$. There are thus no significant geometric nonlinear effects taking place. In order to estimate the modal parameters correctly, the data record was partitioned into short blocks with 50% overlap. The block length is a compromise between sufficient information content and a maximal acceptable modal parameter variation. Under the last assumption, we may use LTI system identification methods.

The free-decay data was identified with the LogDec and the data-driven SSI methods. The sensors nearest to the blade root and the z-direction channels have been excluded due to bad SNR. Figure 8 compares the eigenfrequency and damping ratio over time as estimated by LogDec and data-driven SSI. The latter is paired with the mode tracking technique described in [5] to produce clean tracking diagrams and to isolate the excited eigenmode. Despite LogDec's lesser degree of sophistication, it delivers virtually the same estimates as SSI. Result quality degrades when the amplitude is low because of noise. The damping ratio over time displays a monotone trend, while the eigenfrequency varies much less. The damping ratio of the first three modes (flap 1, edge 1 and flap 2) varies, respectively, by a factor of approximately 4.5, 1.1 and 1.7. The second edge mode and the third flap modes have worse estimates; this may be attributed to the difficulty in exciting them by hand (low vibration amplitude). In figure 9 the damping ratio and eigenfrequency are plotted as a function of vibration RMS. The eigenfrequency decreases by less than 0.5% in relative terms, but it is still possible to resolve a monotone trend. Figure 10 displays the actual difference in damping ratio (in percent of the critical damping) as estimated from the free-decay data and from the hammer test. The hammer test has very low displacements and its estimate compares well to the free-decay results with low amplitudes.

6. CONCLUSIONS

The first five eigenmodes of a wind turbine rotor blade (length: 50.5 m) were identified from ambient excitation, hammer and free-decay tests. Results are compared with current SSI and LSCF methods. Given the low eigenfrequencies of the structure, it was possible to excite it by hand to perform a free-decay test and to estimate the modal parameters using the logarithmic decrement method.

The damping ratio displays a clear and significant monotone dependency on oscillation amplitude, while the eigenfrequency is much less impacted. For low oscillation amplitudes, the estimated damping is comparable to the hammer test results.

We show that with the free-decay procedure the logarithmic decrement approach provides results that are consistent with standard and more sophisticated modal analysis techniques. This approach requires only the output data of the accelerometers and less complex algorithms.

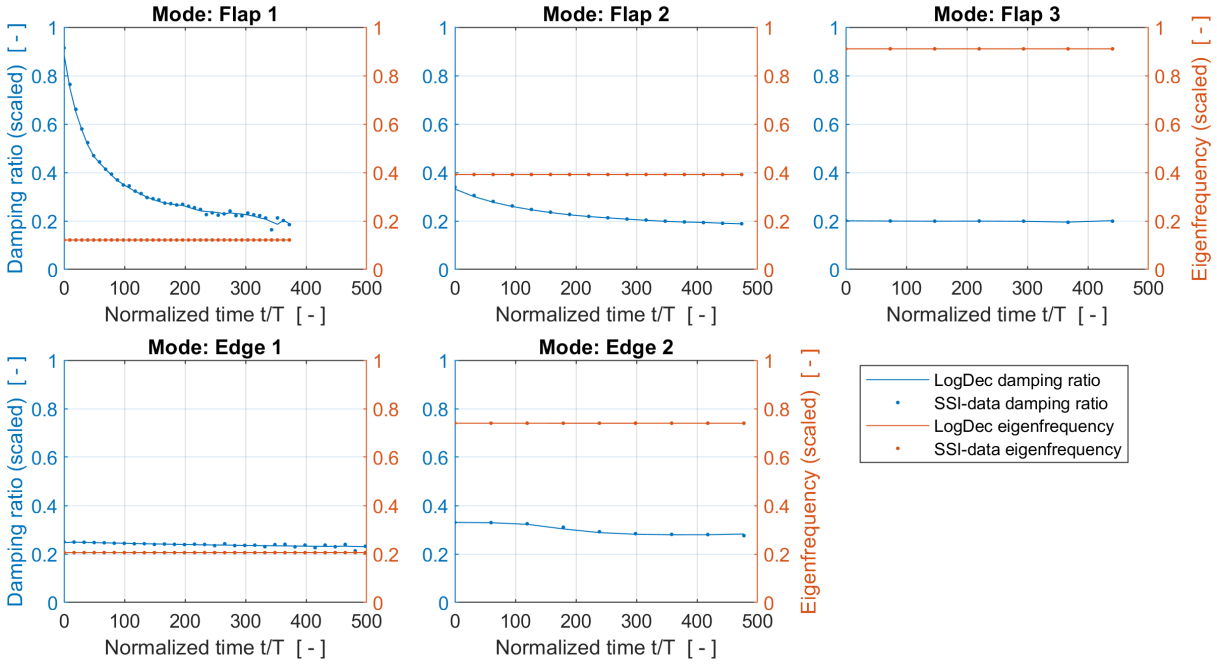

Figure 8: Free-decay data: comparison between the logarithmic decrement and data-driven SSI estimates. The time axis is scaled by the oscillation period T of each eigenmode. The eigenfrequency increases monotonically by less than 0.5% (see detail in figure 9). LogDec estimates are from the IPC accelerometer with the largest RMS.

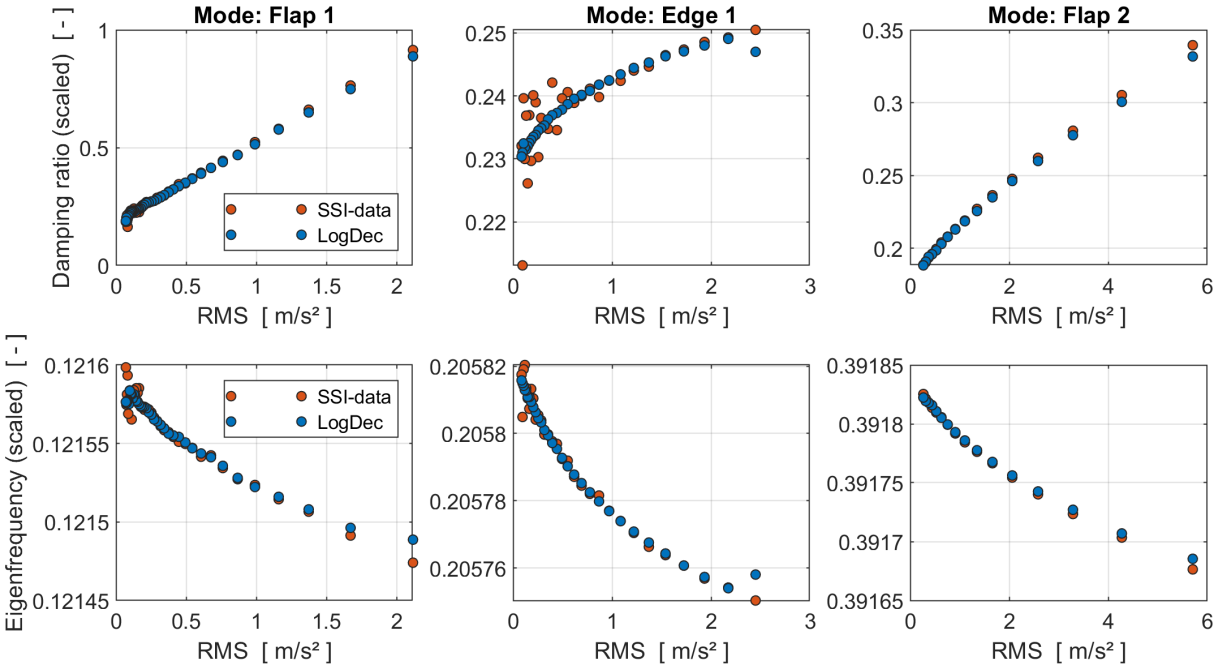

Figure 9: Free-decay data: damping ratio and eigenfrequency as a function of oscillation amplitude. Comparison between the logarithmic decrement and the data-driven SSI. See text for discussion.

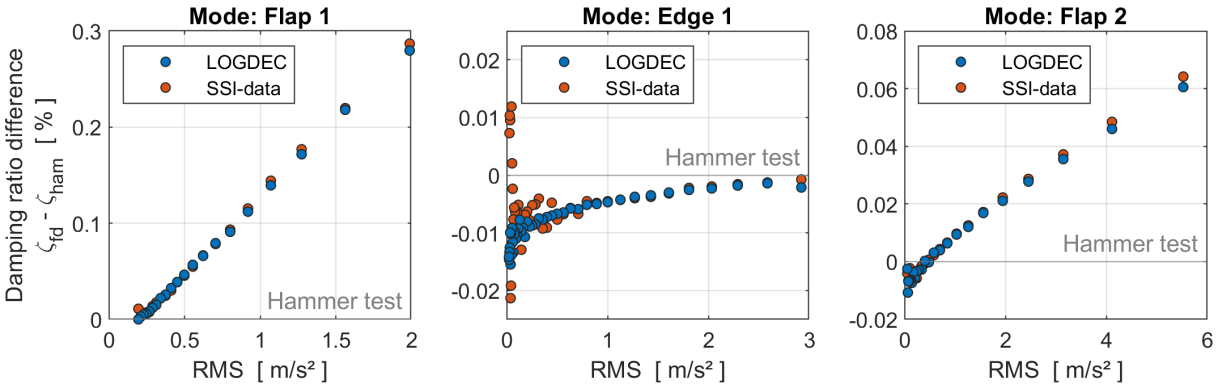

Figure 10: Actual difference of the damping ratio estimates (in percent of the critical damping) between the free-decay and the hammer test. The free-decay estimates are from the data-driven SSI and logarithmic decrement methods. Hammer test results are obtained from significantly lower vibration amplitudes using LSCF.

	Ambient excitation (OMA, SSI)		Hammer test (EMA, LSCF)	
Mode	Eigenfrequency	Damping ratio	Eigenfrequency	Damping ratio
	[-]	[-]	[-]	[-]
1	0.122	0.194	0.122	0.135
2	0.206	0.318	0.206	0.249
3	0.392	0.244	0.392	0.217
4	0.740	0.314	0.740	0.282
5	0.911	0.203	0.911	0.210

Table 1: Comparison between the hammer test (EMA, LSCF) and the ambient excitation (OMA, SSI-data) system identification results. Both data records have low overall oscillation amplitudes. The table reports the scaled damping - the actual difference is less than one percent of the critical damping.

CONTRIBUTION ROLES

Y. Govers: conceptualization, investigation, writing; **K. Gnebner**: investigation; **P. Kober**: investigation; **G. Jelicic**: software, formal analysis, visualization, writing;

REFERENCES

[1] J. Gundlach and Y. Govers. Experimental modal analysis of aeroelastic tailored rotor blades in different boundary conditions. *Journal of Physics: Conference Series*, 1356(012023), October 2019.

[2] J. Gundlach, J. Knebusch, Y. Govers, and B. Haller. Model-based displacement estimation of wind turbine blades using strainmodal data. *Journal of Physics: Conference Series*, 1618(052069), September 2020.

[3] C. Rainieri and Giovanni Fabbrocino. *Operational Modal Analysis of Civil Engineering Structures, An introduction and a guide for applications*. Springer Nature, 2014. ISBN 978-1-4939-0767-0. doi: 10.1007/978-1-4939-0767-0.

[4] E. Reynders, R. Pintelon, and G. De Roeck. Uncertainty bounds on modal parameters obtained from stochastic subspace identification. *Mechanical Systems and Signal Processing*, 22(4):948–969, 2008. doi: https://doi.org/10.1016/j.ymssp.2007.10.009.

[5] G. Jelicic. *System Identification of Parameter-Varying Aeroelastic Systems using Real-Time Operational Modal Analysis*. PhD thesis, Syddansk Universitet (SDU), 2022.

[6] P. Verboven, P. Guillaume, B. Cauberghe, S. Vanlanduit, and E. Parloo. Stabilization Charts and Uncertainty Bounds for Frequency-domain Linear Least Squares Estimators. In *Proceedings of the 21st International Modal Analysis Conference, Kissimmee, Orlando, FL (USA), February 3-6*, 2003.

[7] Y. Liao and V. Wells. Modal parameter identification using the log decrement method and band-pass filters. *Journal of Sound and Vibration*, 330(21), October 2011. doi: 10.1016/j.jsv.2011.05.017.

[8] A.G. Egorov, A.M. Kamalutdinov, and A.N. Nuriev. Evaluation of aerodynamic forces acting on oscillating cantilever beams based on the study of the damped flexural vibration of aluminium test samples. *Journal of Sound and Vibration*, 421:334–347, May 2018. doi: 10.1016/j.jsv.2018.02.006.

[9] A. Agneni and L. Balis-Crema. Damping measurements from truncated signals via hilbert transform. *Mechanical Systems and Signal Processing*, 3(1):1–13, 1989. ISSN 0888-3270. doi: https://doi.org/10.1016/0888-3270(89)90019-8.